tive strangeness equal to -0.6 and -0.1, respectively. If these same parameters are applied to Be the computed phase is less negative by 9°. If, in addition, the momentum is reduced with no change in the relative value of the real parts, the computed phase shifts another $+11°$, giving a total phase shift of $+20°$. Since at the lower momenta a resonance is approached, it is entirely reasonable that the remaining discrepancy arises from a change in the ratios of real to imaginary amplitudes, to which the regeneration phase is highly sensitive.

[21]G. Neuhofer, F. Niebergall, M. Regler, H. E. Stier, K. Winter, J. J. Aubert, X. DeBouard, V. Lepeltier, L. Massonet, H. Pessard, M. Vivargent, T. R. Willitts, M. Yvert, W. Bartl, and M. Steuer, in *Proceedings of the Amsterdam International Conference on Elementary Particles, 1971*, edited by A. G. Tenner and M. Veltman (North-Holland, Amsterdam, 1972).

[22]C. Alff-Steinberger, W. Heuer, K. Kleinknecht, C. Rubbia, A. Scribano, J. Steinberger, M. J. Tannenbaum, and K. Tittel, Phys. Letters 20, 207 (1966); 21, 595 (1966).

[23]H. Faissner, H. Foeth, A. Staude, K. Tittel, P. Darriulat, K. Kleinknecht, C. Rubbia, J. Sandweiss, M. I. Ferrero, and C. Grosso, Phys. Letters 30B, 204 (1969).

Inelastic K^+p Reactions at Incident Momenta from 1.37 to 2.17 GeV/c*

S. C. Loken,† B. C. Barish, and R. Gomez

California Institute of Technology, Pasadena, California 91109

and

D. W. Davies,‡ P. E. Schlein, and W. Slater

University of California, Los Angeles, California 90024

(Received 3 February 1972)

Inelastic K^+p reactions have been studied in a 400 000-picture exposure of the LRL 25-in. hydrogen bubble chamber. Cross sections have been obtained for single-pion and two-pion final states corresponding to the two-prong-V and four-prong topologies. These channels show a smooth energy dependence, consistent with observations at other momenta. The production and decay angular distributions for the quasi-two-body channels agree with the predictions of simple exchange models and show no evidence of an s-channel resonance. It is not possible, however, to place any quantitative limit on the production of a Z^*. Quark-model relations for double-resonance production have been tested and are well satisfied by our data.

I. INTRODUCTION

A number of recent experiments have suggested a possible Z^* resonance in K^+p scattering. The energy dependence of the total K^+p cross section[1] and of the total elastic cross section[2] are shown in Fig. 1. The total elastic cross section falls smoothly with momentum, but the total cross section data show a bump at 1.35 GeV/c and a shoulder at about 1.9 GeV/c. A fit to the bump suggests a resonance of 4 mb at a mass of 1910 MeV. The full width at half-height is 180 MeV and the value of $(J+\frac{1}{2})K$ is 0.3, where J is the spin and K is the elasticity. The shoulder corresponds to a 0.2-mb enhancement at 2190 MeV with a width of 120 MeV and $(J+\frac{1}{2})K = 0.03$.

Analysis of the elastic differential cross section and polarization data also suggests a possible resonance.[3] Some of the solutions from both energy-dependent and energy-independent partial-wave analyses suggest a resonance in the $P_{3/2}$ partial wave at an incident momentum between 1.3 and 1.9 GeV/c. These analyses show that the resonance, if it exists, is very inelastic (elasticities vary between 0.1 and 0.45). They also indicate, however, that the speed (the rate of change of phase shift with energy) is not consistent with resonance behavior.

All experiments which show some resonance features share the common characteristic of a small elasticity. For this reason it is of interest to study the inelastic channels in the K^+p system. In an earlier experiment Bland et al.[4] studied single-pion production at incident momenta between 0.84 GeV/c and 1.37 GeV/c. He concluded that the first bump in the total cross section can be interpreted as a threshold effect, resulting from the opening of the inelastic channel $K\Delta$. There is no indication of a Z^* resonance over the momentum range of that experiment.

It is the purpose of this experiment to extend to higher energies the study of the inelastic K^+p reac-

tions. The lowest momentum 1.37 GeV/c overlaps the data of Bland. The maximum momentum is above any of the reported resonance features.

In this experiment we have studied single-pion and two-pion production. Cross sections have been determined for final states corresponding to four-prong and two-prong-V topologies. Quasi-two-body processes contribute significantly to the pion-production reactions and much of the analysis is devoted to these states. The production and decay of these channels are discussed below and are compared with data from other experiments at higher and lower momenta.

II. DESCRIPTION OF THE EXPERIMENT

A. Beam

The experiment consisted of 400 000 pictures taken in the Lawrence Radiation Laboratory 25-in. hydrogen bubble chamber. The exposure was distributed over seven K^+ momenta, spaced between 1.37 and 2.17 GeV/c.

The K^+ beam was produced at a platinum target in the Bevatron external proton beam and was transported to the bubble chamber in the Bevatron beam $K9$.[5] The momentum was restricted to about $\pm 1\%$ by slits at the first horizontal focus. Two stages of mass separation, each consisting of an electrostatic separator and slits at the vertical focus, were used to remove most of the pions.

A Freon 12 gas threshold Čerenkov counter was installed in the quadrupole magnet directly in front

of the bubble chamber. This counted pions at all momenta except 1.37 and 1.52 GeV/c and gave us a continuous monitor of beam contamination. The pion flux was about 5% of the beam at 2.17 GeV/c, but was less than 2% at all momenta below 1.94 GeV/c.

B. Measuring and Fitting

The film was simultaneously scanned and measured on SMP's (scanning and measuring projectors) at UCLA. We have rescanned about half the film at each momentum and have compared the results of the two scans frame by frame to determine the scanning efficiency. The average inefficiency was 5% and showed no systematic dependence on momentum or topology.

The measured events were processed through the TVGP-SQUAW-ARROW system of programs.[6] Events which were not successfully fit were remeasured and refitted. The failing events have been studied in detail and appear to be random losses. A correction has been applied to all measured cross sections for these failures.

C. Cross-Section Determination

The inelastic reactions discussed in this paper correspond to the two-prong-V and four-prong topologies. At the same time we have measured the three-prong τ decays. These have been used to normalize all cross sections in this paper.

To check this normalization we have done a random track count of each momentum. We have also made a total cross section scan, counting all topologies and comparing to the total cross section known from counter experiments. Both these were in excellent agreement with the primary normalization.

III. SINGLE-PION AND TWO-PION PRODUCTION

A. $pK^0\pi^+$ Final State

In this experiment we have studied only one single-pion reaction,

$$K^+p \to pK^0\pi^+ . \qquad (1)$$

The total cross sections for this final state are presented in Table I and in Fig. 2. The data from previous experiments[4,7] are also shown in the figure. As already pointed out by Bland,[4] the cross section rises sharply with momentum from 0.8 GeV/c and reaches a peak at about 1.3 GeV/c, very close to the bump noted earlier in the total cross section. Above 1.4 GeV/c there is a smooth falloff with momentum suggested by earlier experiments and confirmed by our data over this momentum range.
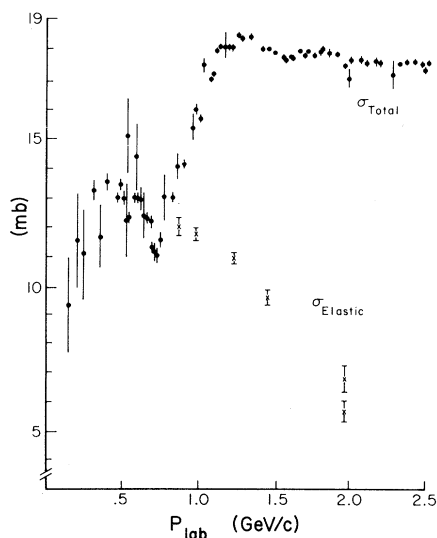

FIG. 1. The energy dependence of the total K^+p cross section (Ref. 1) and the total elastic cross section (Ref. 2).

TABLE I. Cross sections for the reaction $K^+p \to pK^0\pi^+$. A correction has been included for unobserved K^0 decays.

Momentum (GeV/c)	$\sigma(K^+p \to K^0 p\pi^+)$ (mb)
2.17	3.06 ± 0.31
2.07	3.21 ± 0.25
1.94	4.09 ± 0.35
1.81	4.29 ± 0.33
1.67	4.54 ± 0.40
1.52	5.52 ± 0.37
1.37	5.85 ± 0.61

We have also shown in Fig. 2 the cross sections for the other single-pion channels not measured in this experiment,

$$K^+p \to pK^+\pi^0 \tag{2}$$

$$\to nK^+\pi^+ . \tag{3}$$

The features of the $KN\pi$ cross section have been obtained by summing smooth curves drawn through the partial cross sections.

The threshold for single-pion production is at an incident K^+ laboratory momentum of 0.52 GeV/c. The $KN\pi$ cross section is very small, however, until about 0.8 GeV/c, the threshold for production of the quasi-two-body channel $K\Delta$. In Sec. IV we will return to the analysis of the quasi-two-body channels.

B. Two-Pion Production

In this experiment we have measured three reactions having two pions in the final state:

$$K^+p \to pK^+\pi^+\pi^- \tag{4}$$

$$\to pK^0\pi^+\pi^0 \tag{5}$$

$$\to nK^0\pi^+\pi^+ . \tag{6}$$

The cross sections are presented in Table II and are shown in Fig. 3 with data at other momenta.[8]

The threshold for two-pion production at an incident K^+ laboratory momentum is at 0.82 GeV/c, whereas the threshold for the quasi-two-body chan-
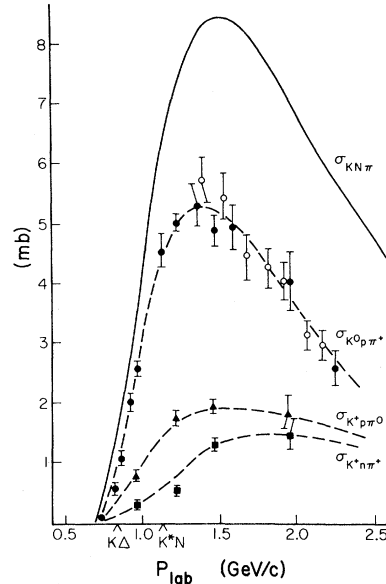

FIG. 2. The energy dependence of single-pion production cross sections. The charge states are indicated by: $K^0p\pi^+$, ●; $K^+p\pi^0$, ▲; $K^+n\pi^+$, ■. The open symbols refer to this experiment, the solid to Refs. 4 and 7. All cross sections for reactions with final state K^0's are corrected for undetected decays.

nel $K^*\Delta$ is at 1.74 GeV/c. The data suggest that this channel contributes very strongly to the two-pion reactions. The details of the quasi-two-body reactions will be discussed in Sec. IV.

IV. QUASI-TWO-BODY REACTIONS

A. Single-Pion Production

The experiment of Bland et al.[4] indicated the dominance of the quasi-two-body channels at lower momenta. The Dalitz plot shown in Fig. 4 suggests the presence of both these channels at the momenta of this experiment.

The cross sections for these channels have been determined from the Dalitz plot density. We have used the mass-conjugation technique[9] to eliminate the possible interference of the two channels in the

TABLE II. Two-pion production total cross sections. Cross sections for K^0 final states are corrected for unseen decays.

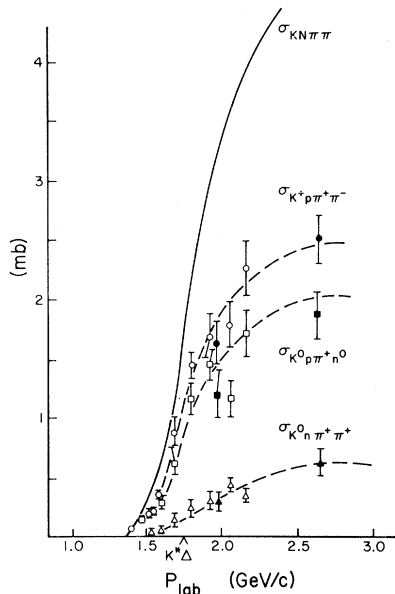| Momentum (GeV/c)	$\sigma(K^+p \to K^+p\pi^+\pi^-)$ (mb)	$\sigma(K^+p \to K^0p\pi^+\pi^0)$ (mb)	$\sigma(K^+p \to K^0n\pi^+\pi^+)$ (mb)
2.17	2.28 ± 0.16	1.75 ± 0.2	0.38 ± 0.06
2.07	1.82 ± 0.11	1.19 ± 0.15	0.43 ± 0.06
1.94	1.72 ± 0.12	1.50 ± 0.17	0.32 ± 0.04
1.81	1.47 ± 0.09	1.20 ± 0.15	0.26 ± 0.04
1.67	0.88 ± 0.07	0.64 ± 0.09	0.17 ± 0.04
1.52	0.24 ± 0.08	0.26 ± 0.05	0.04 ± 0.02
1.37	0.09 ± 0.03	0.12 ± 0.03	0.04 ± 0.02

FIG. 3. The energy dependence of two-pion produc-
tion total cross sections. The charge states are in-
dicated as follows: $K^+p\pi^+\pi^-$, ●; $K^0p\pi^+\pi^0$, ■; $K^0n\pi^+\pi^+$,
▲. The open symbols refer to this experiment, solid
to Ref. 8.

FIG. 4. Dalitz plot for the reaction $K^+p \to pK^0\pi^+$ at
1.52 GeV/c.

region where the two bands cross in the Dalitz plot.
The results are given in Tables III and IV and are
shown in Fig. 5, with data from other experiments.[7]

The behavior of the $KN\pi$ cross section is clearly
dominated by these two reactions, not only in the
threshold region but at higher momenta as well.
At 2.5 GeV/c it appears that the two channels ac-
count for about 80% of the single-pion production.

We have estimated, using the mass conjugation
technique, the $K^*\Delta$ interference contribution to the
$K\pi N$ cross section. The results are shown in Ta-
ble V. The data do show some consistent evidence
of constructive interference although the accuracy
at each momentum is not good. Our results are in
at least qualitative agreement with the data of
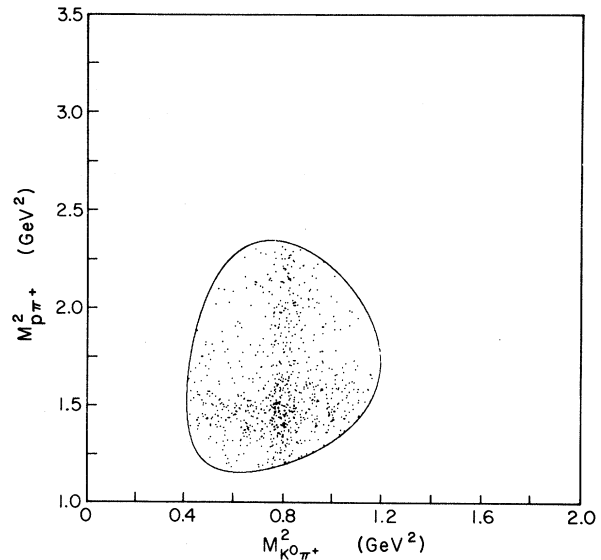Bland[4] at 1.2 and 1.37 GeV/c.

B. Two-Pion Production

From this experiment we can get new information
on the threshold behavior of the reaction

$$K^+p \to K^*(890)\Delta(1236). \tag{7}$$

We will consider in this discussion only reaction
(4), since this accounts for 50% of the $K^*\Delta$ produc-
tion. It is the four-constraint fit for our four-
prong sample and is most free of fitting ambigu-
ities.

Figure 6 shows a plot of $p\pi^+$ effective mass ver-
sus $K^+\pi^-$ effective mass. The cross sections for
the reaction

$$K^+p \to K^{*0}\Delta^{++} \to K^+\pi^-p\pi^+ \tag{8}$$

have been obtained from the effective mass plots
(see Table VI), using a smooth estimate for the
phase-space background.

In Fig. 7 we show all available data for $K^*\Delta$ pro-

TABLE III. Cross sections for $K\Delta$ production. The cross section for $K^+p \to K\Delta$ is obtained
from the reaction $K^+p \to K^0\Delta^{++}$ using Clebsch-Gordan coefficients.

Momentum (GeV/c)	$\sigma(K^+p \to K^0\Delta^{++})$ (mb)	$\sigma(K^+p \to K\Delta)$ (mb)
2.17	1.13± 0.17	1.51± 0.23
2.07	1.27± 0.19	1.70± 0.25
1.94	1.53± 0.23	2.04± 0.30
1.81	1.86± 0.27	2.48± 0.36
1.67	1.92± 0.35	2.56± 0.47
1.52	2.22± 0.39	2.95± 0.52
1.37	3.14± 0.46	4.18± 0.61

TABLE IV. Cross sections for K^*N production.

Momentum (GeV/c)	$\sigma(K^+p \to K^{*+}p)$ (mb)	$\sigma(K^+p \to K^*N)$ (mb)
2.17	0.92 ± 0.14	1.38 ± 0.21
2.07	1.11 ± 0.18	1.66 ± 0.27
1.94	1.30 ± 0.20	1.94 ± 0.30
1.81	1.46 ± 0.21	2.19 ± 0.31
1.67	1.52 ± 0.25	2.28 ± 0.37
1.52	1.88 ± 0.29	2.82 ± 0.43
1.37	2.02 ± 0.32	3.02 ± 0.47

duction up to 2.5 GeV/c, along with the $KN\pi\pi$ cross section estimate from Fig. 2. The $K^*\Delta$ production is seen to be a major contributor to two-pion production over the momentum range covered.

C. K^+p Total Cross Section

In Fig. 8 we review the partial cross sections presented earlier. The sum of these smooth curves reproduces the measured total cross sections reasonably well up to 2.0 GeV/c, where other inelastic reactions become important, and seems to account for the features observed earlier.

The first bump in the total cross section has been studied in detail by Bland,[4] who finds no evidence for a resonance in this momentum range. He concludes that the structure is completely explainable as being due to the onset of the inelastic channels.
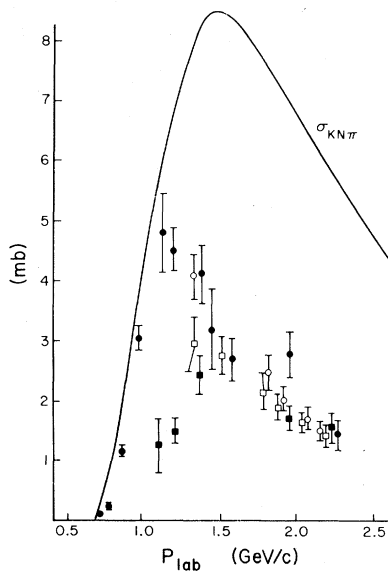

FIG. 5. Cross sections for $K\Delta$ and K^*N production. Data for $K\Delta$ are shown by ● and ○; K^*N by ■ and □. The open symbols refer to this experiment, solid to Ref. 7. The solid line is a smooth estimate to the $KN\pi$ cross section from Fig. 2.

The second bump in the total cross section appears just above the rapid rise of the $KN\pi\pi$ cross section and suggests very strongly that this structure is also a threshold effect.

V. PRODUCTION AND DECAY ANGULAR DISTRIBUTIONS

A. General Discussion

The production and decay of resonances in quasi-two-body reactions can provide very useful information about the reaction mechanism for the process. In the case of the reactions studied in this experiment, considerable information has already been accumulated at higher energies indicating the dominance of peripheral mechanisms. The data of Bland on single-pion production show the dominance of exchange processes at momenta down to threshold.

The dominance of peripheral mechanisms is not, however, inconsistent with the existence of direct-channel resonances. The two descriptions are in fact complementary, and are related in an average way by finite-energy sum rules. The presence of a Z^*, then, would give some local variation about the average contribution from the peripheral mechanism. Such an effect is already known to be small and is very difficult to analyze quantitatively.

The data on reactions where resonances are known to be important can serve as guidelines in our discussion of the K^+p scattering. For example the reaction

TABLE V. Contribution to the $pK^0\pi^+$ final state from $K^*\Delta$ interference. The cross sections have been estimated using the mass conjugation technique on the Dalitz-plot density.

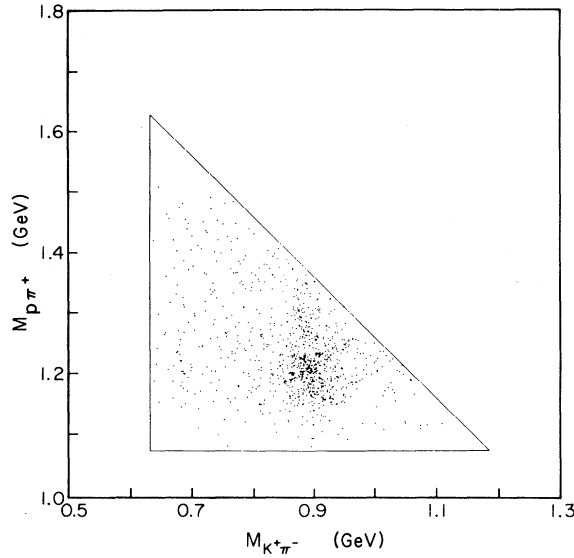| Momentum (GeV/c)	Cross section (mb)
2.17	+0.15 ± 0.07
2.07	−0.04 ± 0.08
1.94	+0.31 ± 0.11
1.81	+0.12 ± 0.08
1.37	+0.16 ± 0.17

FIG. 6. Plot of $p\pi^+$ effective mass as $K^+\pi^-$ effective mass at 2.07 GeV/c.

$$\pi^+ p \to \pi^0 \Delta^{++} \tag{9}$$

is analogous to our reaction

$$K^+ p \to K^0 \Delta^{++}. \tag{10}$$

Reaction (9) has been studied over approximately the same momentum range as this experiment.[10] The differential cross section shows clearly the effect of the dominant $F_{37}(1950)$ partial wave at momenta about 1.5 GeV/c. A Legendre polynomial fit made to the angular distribution shows that the coefficient A_6 becomes large and negative in this range. The odd coefficients A_5 and A_7 change sign at about 1.5 GeV/c indicating a rapid phase change in the dominant amplitude.

The $F_{37}(1950)$ resonance is known from elastic phase-shift analysis. It has a rather small elasticity (0.4) and a branching fraction into $\pi\Delta$ of about 50%. In addition, the high spin enhances the effect both because of the factor $(J+\tfrac{1}{2})$ and because the contribution to the Legendre expansion is in the highest-order terms.
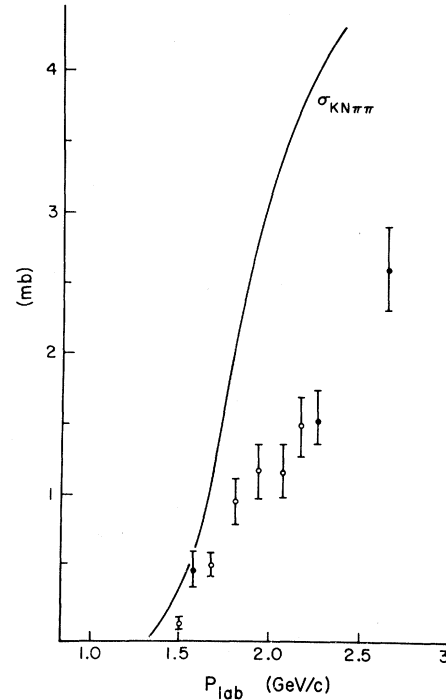

FIG. 7. Cross sections for $K^*\Delta$ production. The open symbols refer to this experiment, solid to Ref. 13. The solid curve is a smooth estimate of the $KN\pi\pi$ cross section.

It is much more difficult to see the effect of resonances in lower partial waves. Since any partial wave with angular momentum L contributes to Legendre coefficients of order $2L$ and less, a good knowledge of the highest partial waves is required to separate the effect of any lower wave. This information has come in most analyses from the phase-shift analyses of the elastic scattering data.[11]

The Kp system in this momentum range is very similar kinematically to the πp case and allows the same partial waves. The best candidate for a Z^*, however, is the P_{13} partial wave. The fact that this is such a low partial wave makes it extremely difficult to answer the question of the existence of the

TABLE VI. Cross sections for the reaction $K^+p \to K^{*0}\Delta^{++} \to K^+\pi^- p\pi^+$ and for $K^+p \to K^*\Delta$ calculated using isospin conservation.

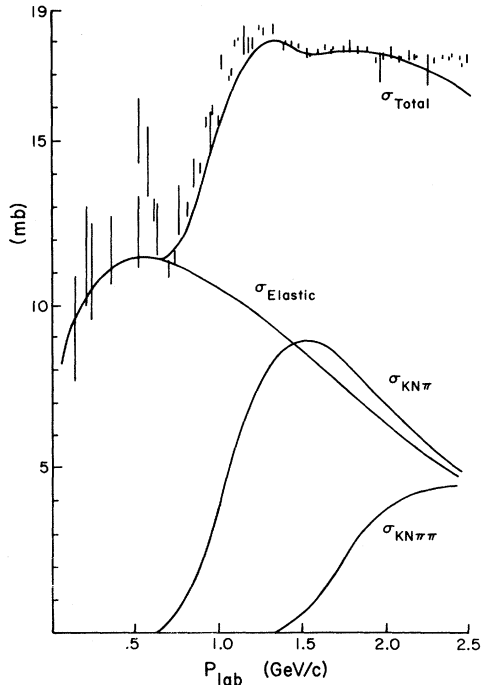| Momentum (GeV/c)	$\sigma(K^+p \to K^{*0}\Delta^{++} \to K^+\pi^- p\pi^+)$ (mb)	$\sigma(K^+p \to K^*\Delta)$ (mb)
2.17	0.77 ± 0.12	1.53 ± 0.23
2.07	0.61 ± 0.09	1.21 ± 0.18
1.94	0.59 ± 0.09	1.18 ± 0.18
1.81	0.49 ± 0.08	0.97 ± 0.15
1.67	0.29 ± 0.04	0.57 ± 0.08
1.52	0.06 ± 0.04	0.12 ± 0.08
1.37	0	0

FIG. 8. K^+p partial cross sections. The energy dependence of the total elastic, single-pion and two-pion cross sections are shown by smooth curves. The sum of these is compared with measurements of the total cross sections from Ref. 1.
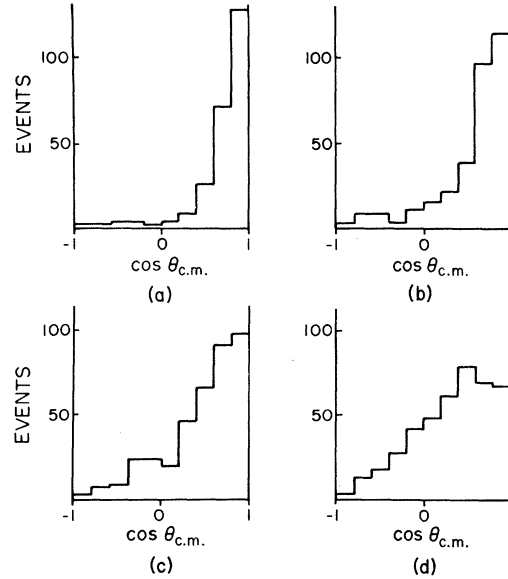

FIG. 9. Production angular distributions for the reactions $K^+p \rightarrow K^0\Delta^{++}$ at four momenta: (a) 2.17 GeV/c, (b) 1.94 GeV/c, (c) 1.67 GeV/c, (d) 1.37 GeV/c. $\theta_{c.m.}$ is the angle of the Δ^{++} measured with respect to the incoming proton.

Z^* from the inelastic channels alone. Good knowledge of the inelastic differential cross sections can, however, provide additional constraints for the partial-wave analyses of elastic differential cross sections and polarization, and should help to reduce the number of ambiguous solutions.

In the next sections, we will consider each of the quasi-two-body channels. We use normalized Legendre expansion coefficients to describe the differential cross section at each momentum. Combined with the data of Bland,[4] these provide a complete and model-independent description of the inelastic channels from threshold to 2.2 GeV/c. All suggested resonance phenomena are within this range.

The remainder of the discussion will be in terms of the exchange-model description. Using the spin density matrix elements we can compare our data with data at higher momenta and can study in a qualitative way the mechanisms in each of the quasi-two-body channels.

B. $K^0\Delta^{++}$ Differential Cross Section

The qualitative features of the production angular distribution are shown in Fig. 9, where $\theta_{c.m.}$ is the angle of the Δ measured with respect to the inci-

dent proton in the production center-of-mass system. As expected, the reaction is strongly peaked in the forward direction. This peaking becomes more pronounced as the energy increases.

A quantitative measure of these effects is shown by the energy dependence of the normalized Legendre coefficients

$$W(\cos\theta_{c.m.}) = 1 + \sum_l A_l P_l(\cos\theta_{c.m.}).$$

These are shown in Table VII for the momenta of this experiment. The behavior of the first four coefficients from threshold to 2.17 GeV/c is shown in Fig. 10.

The region up to 1.58 GeV/c has been studied by Bland[4] and the Δ production and decay were found to be in good agreement with the ρ-exchange model of Stodolsky and Sakurai.[12] In particular, the production angular distribution near threshold shows an approximate $\sin^2\theta_{c.m.}$ dependence (corresponding to $A_2 = -1$). At higher momenta the reaction becomes more peripheral as other partial waves become important.

The data from this experiment are in good agreement with that of Bland over the range of overlap and show a smooth variation with incident momentum.

It has been pointed out by Bland that the simple ρ-exchange model fails to explain the magnitude or energy dependence of the differential cross section. The data require very large coupling constants, and

TABLE VII. Coefficients of the normalized Legendre expansion for the $K^+p \to K^0\Delta^{++}$ production angular distribution.

Momentum (GeV/c)	1.37	1.52	1.67	1.81	1.94	2.07	2.17
A_1	0.97 ± 0.06	1.19 ± 0.06	1.40 ± 0.07	1.52 ± 0.07	1.72 ± 0.07	1.77 ± 0.08	2.03 ± 0.07
A_2	-0.22 ± 0.10	0.22 ± 0.09	0.51 ± 0.11	0.83 ± 0.12	1.19 ± 0.11	1.44 ± 0.15	1.97 ± 0.12
A_3	-0.37 ± 0.12	-0.19 ± 0.11	-0.07 ± 0.13	0.06 ± 0.15	0.17 ± 0.14	0.76 ± 0.19	1.03 ± 0.18
A_4	-0.30 ± 0.13	-0.46 ± 0.12	-0.57 ± 0.14	-0.36 ± 0.16	-0.76 ± 0.16	0.05 ± 0.21	-0.14 ± 0.21
A_5	-0.09 ± 0.15	-0.59 ± 0.14	-0.77 ± 0.17	-0.18 ± 0.17	-1.09 ± 0.17	-0.22 ± 0.24	-0.74 ± 0.23
A_6	-0.17 ± 0.17	-0.23 ± 0.15	-0.39 ± 0.19	-0.10 ± 0.19	-1.35 ± 0.19	-0.52 ± 0.25	-0.76 ± 0.25
A_7	-0.16 ± 0.18	0.04 ± 0.16	-0.27 ± 0.19	-0.24 ± 0.20	-1.00 ± 0.21	-0.65 ± 0.29	-0.56 ± 0.27
A_8	-0.11 ± 0.19	-0.13 ± 0.17	-0.29 ± 0.20	-0.44 ± 0.22	-0.35 ± 0.24	-0.66 ± 0.29	-0.40 ± 0.29
A_9	-0.19 ± 0.20	0.04 ± 0.19	-0.03 ± 0.21	-0.55 ± 0.23	-0.11 ± 0.25	-0.48 ± 0.30	-0.05 ± 0.30
A_{10}	0.02 ± 0.21	0.15 ± 0.19	0.53 ± 0.24	0.47 ± 0.25	0.01 ± 0.27	-0.29 ± 0.32	-0.02 ± 0.33

the reaction becomes more peripheral faster than predicted from the simple ρ-exchange hypothesis. The data at higher momenta[13] show a sharp forward peak, explained by absorption of low partial waves, or by a Regge model.

The differential cross sections shown in Fig. 11 show a smooth variation with energy. The data have an approximate e^{at} dependence with a increasing at higher incident momentum. This be-
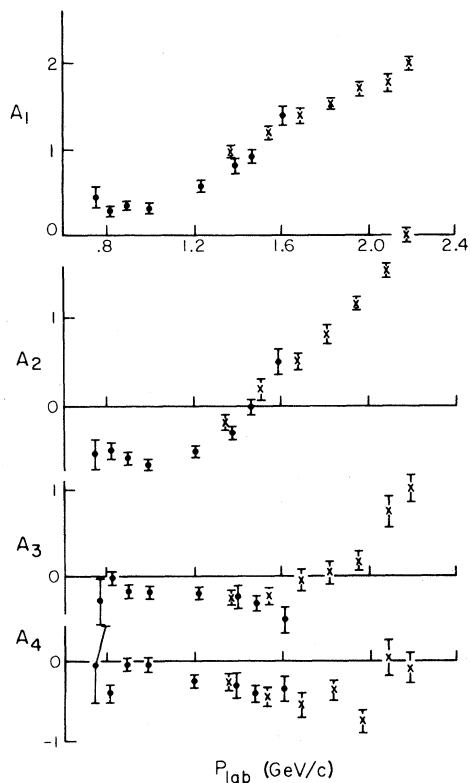

FIG. 10. Legendre expansion coefficients for the production angular distributions in the reaction $K^+p \to K^0\Delta^{++}$. The data from this experiment are shown by ×; that of Bland (Ref. 4) by ●.
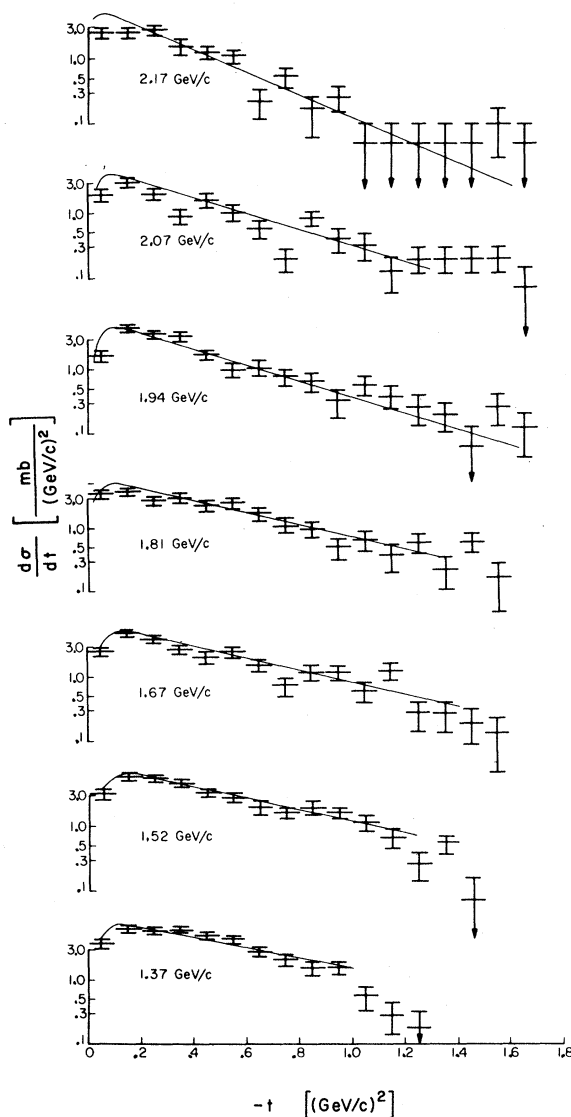

FIG. 11. The differential cross section for the reaction $K^+p \to K^0\Delta^{++}$. The curves are hand drawn. The Δ^{++} mass selection is 1.14–1.29 GeV.
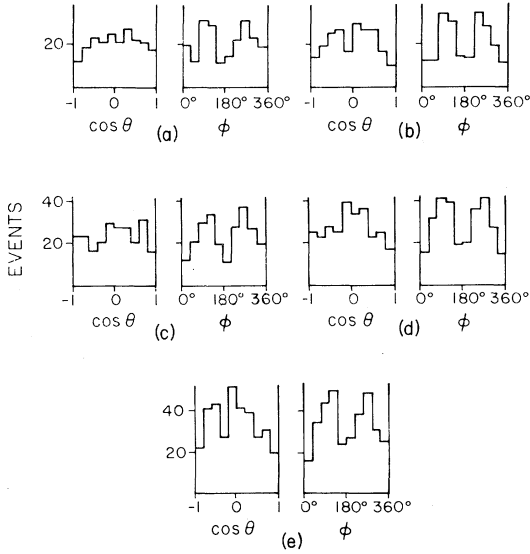
FIG. 12. Δ decay angular distributions for the reactions $K^+ p \to K^0 \Delta^{++} \to K^0 p \pi^+$ at five momenta: (a) 2.17 GeV/c, (b) 2.07 GeV/c, (c) 1.94 GeV/c, (d) 1.81 GeV/c, (e) 1.37 GeV/c. The angles θ and ϕ are measured in the Gottfried-Jackson frame.

FIG. 13. Δ^{++} density matrix elements measured in the Gottfried-Jackson frame. The dashed lines correspond to the $M1$ prediction of Stodolsky-Sakurai discussed in the text. The Δ^{++} mass selection was 1.14–1.29 GeV. No cuts were applied on momentum transfer.

havior is confirmed by measurements at higher momenta. The statistics of this experiment are not sufficient to permit a useful comparison with possible exchange models. In Sec. V C, however, we do consider the relation of the exchange mechanism to the decay angular distribution.

C. Δ-Decay Angular Distribution

We describe the decay of the Δ in the Gottfried-Jackson coordinate frame. The characteristics, shown in Fig. 12, appear to be independent of momentum.

To analyze the momentum dependence in detail, we parametrize the distribution by the spin-$\frac{3}{2}$ density matrix elements. The angular distribution then is given by
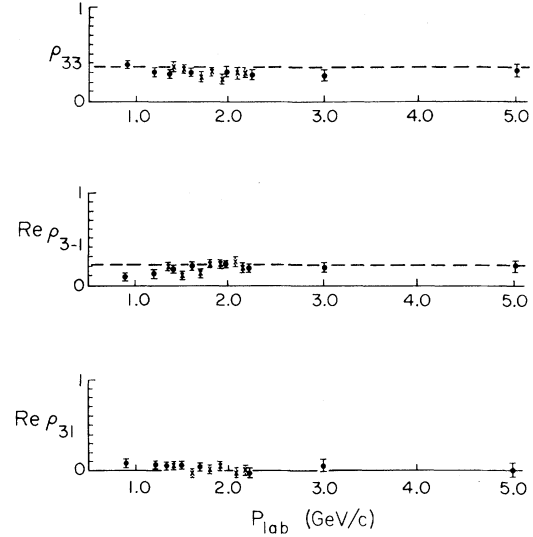
$$W(\cos\theta, \phi) = \frac{3}{4\pi}\left[\rho_{33}\sin^2\theta + \rho_{11}(\tfrac{1}{3} + \cos^2\theta)\right.$$

$$- \frac{2}{\sqrt{3}} \operatorname{Re}\rho_{3-1}\sin^2\theta\cos2\phi$$

$$\left. - \frac{2}{\sqrt{3}} \operatorname{Re}\rho_{31}\sin2\theta\cos\phi\right],$$

where

$$\rho_{33} = \tfrac{1}{2} - \rho_{11}.$$

The values of the density matrix elements have been evaluated from the moments of the angular distribution. The results are shown in Table VIII and are compared, in Fig. 13, with data at other momenta.[7]

TABLE VIII. Density matrix elements for the decay of the Δ^{++} in the reaction $K^+ p \to K^0 \Delta^{++}$ $\to K^0 p \pi^+$. Decay angles are evaluated in the Jackson coordinate frame. The Δ^{++} mass selection used is 1.14–1.29 GeV. No cuts are made on momentum transfer.

Momentum (GeV/c)	ρ_{33}	$\operatorname{Re}\rho_{3-1}$	$\operatorname{Re}\rho_{31}$
1.37	0.379± 0.027	0.230± 0.031	0.059± 0.025
1.52	0.365± 0.028	0.127± 0.030	0.074± 0.026
1.67	0.278± 0.032	0.122± 0.031	0.015± 0.033
1.81	0.329± 0.032	0.245± 0.032	0.016± 0.027
1.94	0.232± 0.037	0.208± 0.033	0.069± 0.031
2.07	0.319± 0.035	0.279± 0.034	−0.033± 0.031
2.17	0.314± 0.036	0.179± 0.037	0.004± 0.034

TABLE IX. Legendre coefficients for the reaction $K^+p \to K^{*+}p$.

Momentum (GeV/c)	1.37	1.52	1.67	1.81	1.94	2.07	2.17
A_1	0.89 ± 0.09	1.16 ± 0.07	1.10 ± 0.08	1.42 ± 0.08	1.64 ± 0.08	1.49 ± 0.10	1.82 ± 0.08
A_2	0.16 ± 0.12	0.48 ± 0.11	0.50 ± 0.12	0.89 ± 0.14	1.27 ± 0.14	1.01 ± 0.15	1.63 ± 0.15
A_3	0.04 ± 0.15	0.12 ± 0.13	0.17 ± 0.15	0.35 ± 0.17	0.66 ± 0.17	0.49 ± 0.19	0.85 ± 0.20
A_4	-0.30 ± 0.16	-0.24 ± 0.15	-0.07 ± 0.17	0.01 ± 0.18	0.08 ± 0.20	-0.14 ± 0.24	0.24 ± 0.24
A_5	-0.14 ± 0.18	-0.36 ± 0.16	0.04 ± 0.19	-0.16 ± 0.10	-0.15 ± 0.22	-0.46 ± 0.26	-0.26 ± 0.26
A_6	0.23 ± 0.20	-0.30 ± 0.18	0.15 ± 0.20	-0.17 ± 0.22	-0.32 ± 0.25	-0.17 ± 0.28	-0.26 ± 0.28
A_7	0.05 ± 0.21	0.10 ± 0.19	0.22 ± 0.22	-0.21 ± 0.24	-0.18 ± 0.27	0.22 ± 0.30	0.12 ± 0.31
A_8	-0.08 ± 0.23	0.23 ± 0.21	0.19 ± 0.22	-0.34 ± 0.26	0.00 ± 0.28	0.39 ± 0.32	-0.02 ± 0.33
A_9	-0.10 ± 0.24	0.01 ± 0.22	-0.18 ± 0.24	-0.34 ± 0.27	0.03 ± 0.30	0.81 ± 0.34	0.03 ± 0.35
A_{10}	-0.22 ± 0.26	-0.09 ± 0.23	0 ± 0.26	-0.61 ± 0.28	0.15 ± 0.32	0.65 ± 0.34	-0.15 ± 0.38

As mentioned previously, the ρ-photon analogy of Stodolsky and Sakurai[12] provides a simple description of the $N\rho\Delta$ coupling. They suggest that the ρ-exchange reactions

$$\pi^+p \to \pi^0\Delta^{++}, \tag{9}$$

$$K^+p \to K^0\Delta^{++} \tag{10}$$

have the same features as Δ photoproduction, which is known to be dominated by an $M1$ transition. The ρ-photon analogy then predicts a decay angular distribution

$$W(\cos\theta, \phi) = \frac{1}{16\pi}\left(2 + 3\sin^2\theta - 3\sin^2\theta\cos2\phi\right).$$

In terms of the density matrix elements the Stodolsky-Sakurai predictions are

$$\rho_{33} = \tfrac{3}{8} = 0.375,$$

$$\mathrm{Re}\rho_{3-1} = \tfrac{1}{8}\sqrt{3} = 0.218,$$

$$\mathrm{Re}\rho_{31} = 0.0.$$

These values are shown in Fig. 13 and appear to be in good agreement with experiment over a wide range of incident momentum.

This result seems to be more general than simple ρ exchange. In contrast to the case of $\pi^0\Delta^{++}$ production, which allows only ρ exchange, the $K^0\Delta^{++}$ state can also be formed by exchange of the A_2. An analysis[14] of the complementary reaction

$$\pi^+p \to \eta\Delta^{++}, \tag{11}$$

which allows only A_2 exchange, also appears to be consistent with the predictions of $M1$ dominance.

The data at higher momenta[13] do show a deviation from the simple $M1$ predictions for $|t| \lesssim 0.1$ (GeV/$c)^2$. Although we have found no consistent variation with momentum transfer, because of the kinematic cutoff in t, we cannot determine values for $|t| < 0.1$.

D. K^*p Differential Cross Section

The production angular distributions for the reaction

$$K^+p \to K^{*+}p \tag{12}$$

show the same qualitative features as previously described for the $K^0\Delta^{++}$ production. The coefficients of the Legendre expansion are given in Table IX. In Fig. 14 we summarize the energy de-
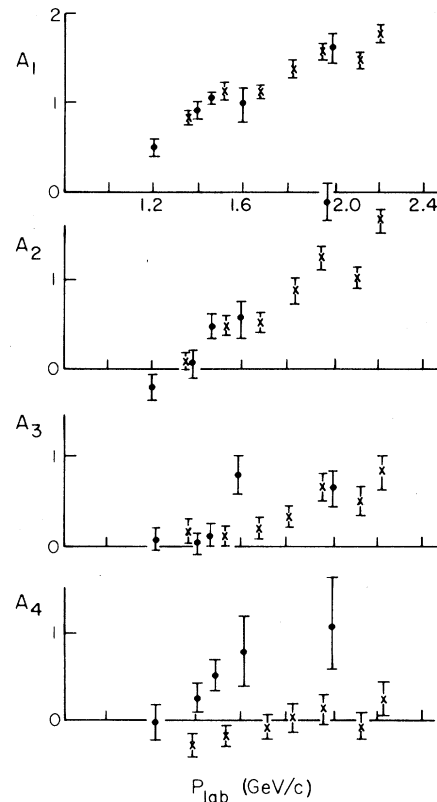

FIG. 14. Legendre expansion coefficients for the reaction $K^+p \to K^{*+}p$. Data are shown from this experiment x and from Ref. 4 ●.
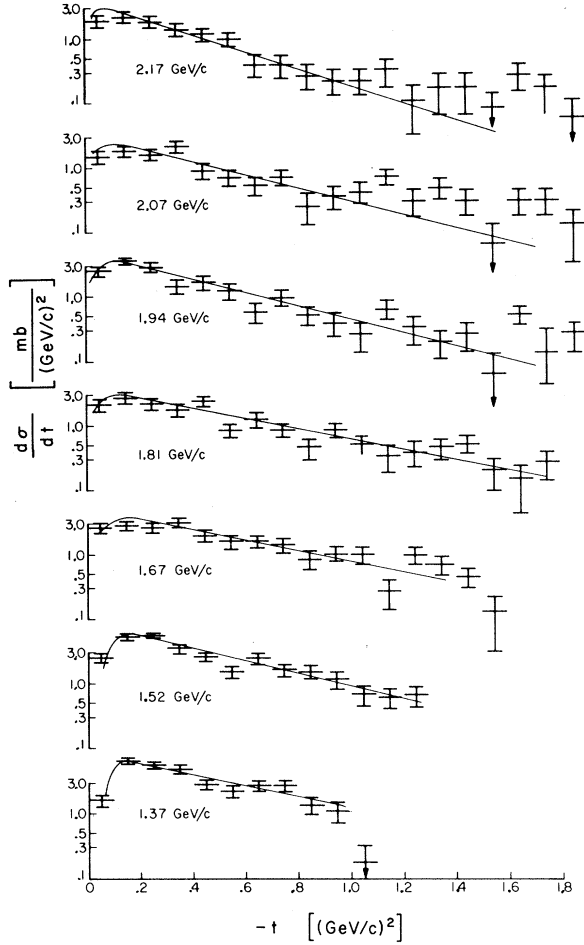
FIG. 15. Differential cross sections for the reaction
$K^+p \to K^{*+}p$. The curves are hand drawn. The K^*
mass selection is 0.84–0.94 GeV.

FIG. 16. Decay angular distributions for the reaction
$K^+p \to K^{*+}p \to K^0\pi^+p$ at five momenta: (a) 2.17 GeV/c,
(b) 2.07 GeV/c, (c) 1.94 GeV/c, (d) 1.81 GeV/c, (e) 1.37
GeV/c. Cos $\theta = (\hat{K}^+ \cdot \hat{K}^0)_{K^*c.m.}$.

pendence of the production angular distribution
from threshold to 2.17 GeV/c. The data confirm
the smooth behavior and the increasingly peripher-
al nature of the reaction.

The differential cross sections shown in Fig. 15
suggest an approximately exponential dependence
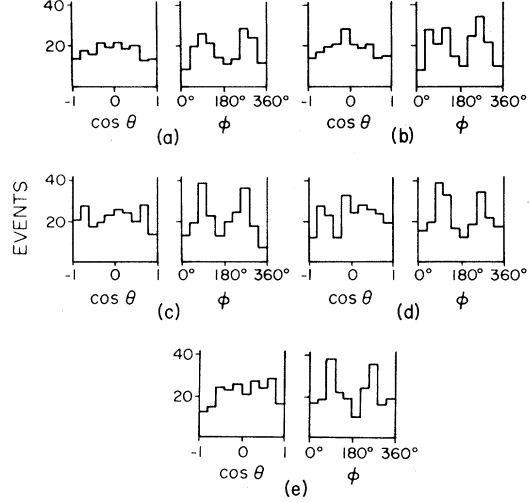on momentum transfer. The slope increases with

energy, in agreement with observations at higher
momentum.[13]

The details of this reaction are more complicated
than the $K^0\Delta^{++}$ production since both natural- and
unnatural-parity exchanges are allowed by angular
momentum-parity conservation. The analysis of
data at higher momentum[13] has shown the dominant
contribution to be from π and ω exchange. The sta-
tistics of this experiment are not sufficiently good
to permit a detailed study of exchange-model pre-
dictions. In Sec. V E, however, we will study the
relative contributions of the exchanges over the
momenta of this experiment.

E. K^{*+} Decay Angular Distribution

The general features of the K^* decay (Fig. 16)
are also very similar to the Δ decay. We again
measure the angles in the Gottfried-Jackson
frames, defined now by the incoming K^+, and we
parametrize the angular distribution in terms of
the spin-1 density matrix elements.

TABLE X. Density matrix elements for the K^* decay in the reaction $K^+p \to K^{*+}p \to K^0\pi^+p$.
The K^* mass selection used is 0.84–0.94 GeV. No cuts are made on momentum transfer.

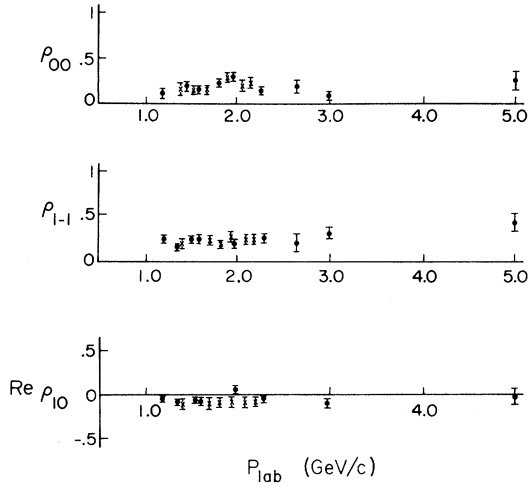| Momentum (GeV/c)	ρ_{00}	ρ_{1-1}	Re ρ_{10}
1.37	0.163 ± 0.039	0.169 ± 0.044	−0.115 ± 0.026
1.52	0.201 ± 0.040	0.228 ± 0.038	0.045 ± 0.021
1.67	0.141 ± 0.042	0.230 ± 0.040	−0.085 ± 0.022
1.81	0.231 ± 0.043	0.176 ± 0.041	−0.051 ± 0.027
1.94	0.286 ± 0.048	0.278 ± 0.041	−0.079 ± 0.028
2.07	0.203 ± 0.047	0.215 ± 0.042	−0.089 ± 0.027
2.17	0.264 ± 0.054	0.244 ± 0.047	−0.075 ± 0.027

FIG. 17. K^* density matrix elements measured in the Gottfried-Jackson frame. Data are shown from this experiment X and Ref. 13 ●. The K^* mass selection is 0.84–0.94 GeV. No cuts were made on momentum transfer.

$$W(\cos\theta, \phi) = \frac{3}{4\pi}\left(\rho_{00}\cos^2\theta + \rho_{11}\sin^2\theta\right.$$

$$- \rho_{1-1}\sin^2\theta\cos2\phi$$

$$\left. - \sqrt{2}\ \mathrm{Re}\rho_{10}\sin2\theta\cos\phi\right),$$

with

$$\rho_{11} = \tfrac{1}{2}(1 - \rho_{00}).$$

The results are given in Table X for the momenta of this experiment. In Fig. 17 we show the values of these density matrix elements from threshold to 5 GeV/c. There seems to be little dependence on momentum over this range.

The two exchange mechanisms π and ω mentioned previously contribute to the density matrix elements ρ_{00} and ρ_{11}, respectively. The relative exchange contributions appear to be independent of
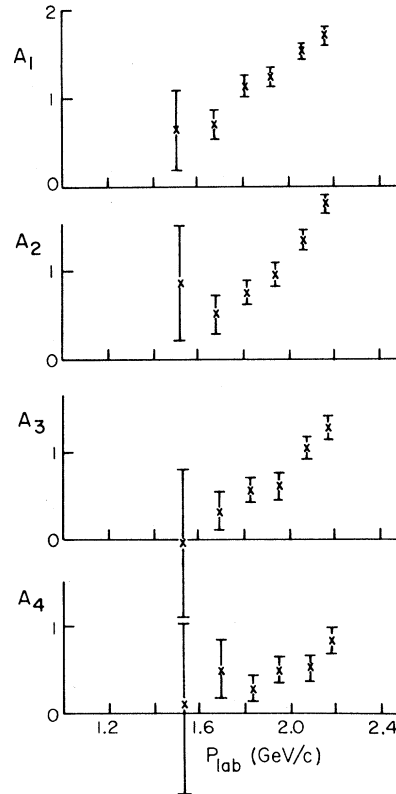

FIG. 18. Legendre expansion coefficients for the reaction $K^+p \to K^{*0}\Delta^{++}$ measured at the six momenta of this experiment.

momentum, in contrast to simple absorption model or Regge predictions. We would expect to see changes particularly at small momentum transfer. However, because of the kinematic cutoff in t our data sample is not sufficient to determine the density matrix elements for small t values.

F. $K^*\Delta$ Differential Cross Section

The qualitative features of the angular distribution are very similar to those of the other chan-

TABLE XI. Legendre coefficients for the reaction $K^+p \to K^{*0}\Delta^{++}$.

| Momentum (GeV/c)	1.52	1.67	1.81	1.94	2.07	2.17
A_1	0.68 ± 0.53	0.68 ± 0.15	1.12 ± 0.08	1.24 ± 0.07	1.51 ± 0.07	1.67 ± 0.06
A_2	0.93 ± 0.66	0.60 ± 0.20	0.77 ± 0.12	0.98 ± 0.11	1.42 ± 0.11	1.79 ± 0.10
A_3	-0.04 ± 0.87	0.30 ± 0.24	0.55 ± 0.15	0.62 ± 0.14	1.00 ± 0.15	1.23 ± 0.13
A_4	0.08 ± 0.95	0.54 ± 0.28	0.23 ± 0.18	0.49 ± 0.16	0.49 ± 0.17	0.82 ± 0.16
A_5	-1.18 ± 1.06	0.29 ± 0.31	0.27 ± 0.20	0.35 ± 0.18	0.32 ± 0.19	0.69 ± 0.18
A_6	0.66 ± 1.03	-0.09 ± 0.34	0.39 ± 0.22	0.34 ± 0.20	0.25 ± 0.21	0.40 ± 0.20
A_7	0.72 ± 0.89	0.27 ± 0.36	0.40 ± 0.23	0.20 ± 0.22	0.24 ± 0.22	0.28 ± 0.22
A_8	-0.14 ± 0.97	0.48 ± 0.40	0.54 ± 0.24	0.27 ± 0.23	0.24 ± 0.23	0.40 ± 0.23
A_9	-1.31 ± 1.24	-0.05 ± 0.43	0.40 ± 0.26	0.05 ± 0.24	0.39 ± 0.25	0.19 ± 0.24
A_{10}	0.80 ± 1.40	0.04 ± 0.44	0.56 ± 0.27	-0.08 ± 0.24	0.23 ± 0.26	0.21 ± 0.24
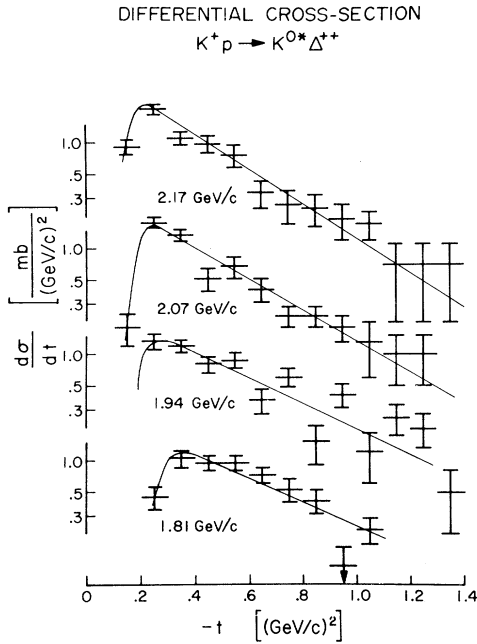
FIG. 19. Differential cross section for the reaction $K^+p \to K^{*0}\Delta^{++}$. The curves are hand drawn. The Δ^{++} and K^* mass cuts are 1.14–1.29 and 0.84–0.94, respectively.
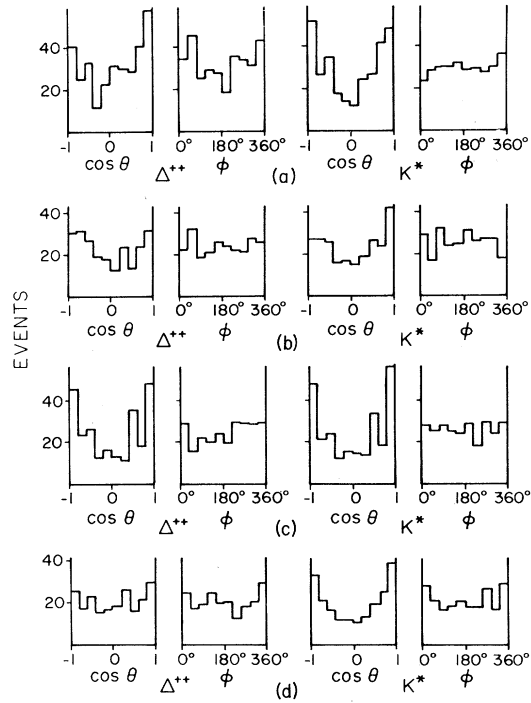

FIG. 20. Decay angular distributions for the reaction $K^+p \to K^{*0}\Delta^{++} \to K^+\pi^-\pi^+p$ at four momenta: (a) 2.17 GeV/c, (b) 2.07 GeV/c, (c) 1.94 GeV/c, (d) 1.81 GeV/c. The angles are measured in the Gottfried–Jackson frame.

nels. This is indicated in the coefficients of the Legendre expansion shown in Table XI, and in Fig. 18. The data again show a very smooth variation, becoming more peripheral at higher momenta.

This reaction has been studied in detail at higher momenta and found in reasonable agreement with models based on π exchange, although none of the models successfully accounts for all features of the data.[15] The differential cross sections shown in Fig. 19 provide new information on the threshold region for this reaction and are in qualitative agreement with expectations from data at higher momenta. We have not made a quantitative comparison with theories but will in the next section discuss the π-exchange interpretation in connection with the K^* and Δ decay angular distributions.

G. K^* and Δ Decay Angular Distributions

The decay cosine and the Treiman-Yang angle are shown in Fig. 20. In contrast to the reactions just studied, there is a very flat distribution in the Treiman-Yang angle ϕ, consistent with the dominance of π exchange. This is in agreement with the data at higher momenta.[15]

We have determined the density matrix elements for both the K^* and Δ (Table XII) and compared the results with data at higher momenta in Fig. 21. The data appear to be rather independent of momentum.

TABLE XII. Density matrix elements for the decay of the K^* and Δ in the reaction $K^+p \to K^{*0}\Delta^{++} \to K^+\pi^-\pi^+p$. The Δ^{++} and K^* mass selections are 1.14–1.29 GeV and 0.84–0.94 GeV, respectively. No cuts are made on momentum transfer.

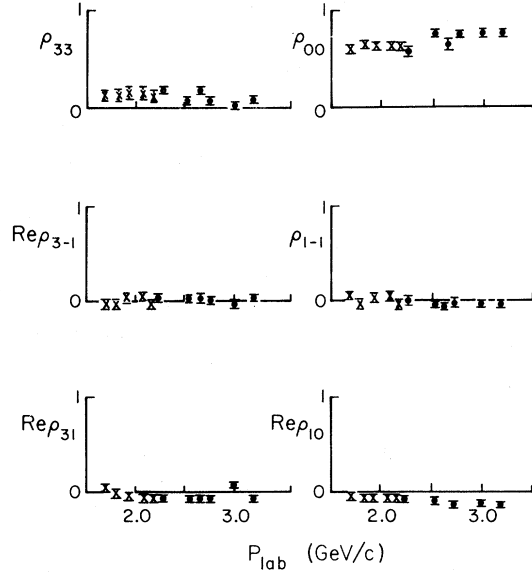| Momentum (GeV/c)	ρ_{33}	Re ρ_{3-1}	Re ρ_{31}	ρ_{00}	ρ_{1-1}	Re ρ_{10}
1.67	0.129 ± 0.043	-0.025 ± 0.042	0.047 ± 0.049	0.599 ± 0.067	0.013 ± 0.044	-0.030 ± 0.037
1.81	0.127 ± 0.029	-0.034 ± 0.026	-0.012 ± 0.029	0.659 ± 0.040	-0.147 ± 0.028	-0.080 ± 0.025
1.94	0.158 ± 0.027	0.014 ± 0.124	-0.127 ± 0.026	0.616 ± 0.037	0.010 ± 0.026	-0.086 ± 0.022
2.07	0.139 ± 0.028	0.037 ± 0.025	-0.031 ± 0.027	0.604 ± 0.037	0.018 ± 0.027	-0.066 ± 0.022
2.17	0.099 ± 0.025	-0.018 ± 0.021	-0.064 ± 0.025	0.619 ± 0.032	-0.030 ± 0.024	-0.048 ± 0.020

FIG. 21. Δ^{++} and K^{*0} density matrix elements measured in the Gottfried-Jackson frame. The Δ^{++} and K^* mass selections are 1.14–1.29 GeV and 0.84–0.94 GeV, respectively. No cuts are made on momentum transfer.

The predictions of simple pion exchange are

$$K^*: \quad \rho_{00}=1, \quad \rho_{1-1}=0, \quad \mathrm{Re}\rho_{10}=0.$$

$$\Delta: \quad \rho_{33}=0, \quad \mathrm{Re}\rho_{3-1}=0, \quad \mathrm{Re}\rho_{31}=0.$$

The density matrix elements, averaged over momentum transfer, do show consistent deviations from these predictions. Although data at higher momenta show that the predictions are better satisfied for small momentum transfer $[\,|t|\lesssim 0.1$ $(\mathrm{GeV}/c)^2]$, our data do not contribute further to this subject.

H. Quark-Model Predictions

Białas and Zalewski[16] have derived a set of relations between single-particle decay angular distributions and joint decay angular distributions for the reaction $K^+p \to K^*\Delta$.

The observable predictions given for decay distributions are presented as predictions for ten-

sors formed from the moments of the angular distributions.

$$T^{20}_{M0}(K^*, \Delta) = \frac{1}{(2 \times \frac{3}{2} + 1)^{1/2} F(K^*)} \langle\, Y^M_2(K^*)\,\rangle,$$

$$T^{02}_{0M}(K^*, \Delta) = \frac{1}{(2 \times 1 + 1)^{1/2} F(\Delta)} \langle\, Y^M_2(\Delta)\,\rangle,$$

$$T^{22}_{MN}(K^*\Delta) = \frac{1}{F(K^*)F(\Delta)} \langle\, Y^M_2(K^*)Y^N_2(\Delta)\,\rangle,$$

$$F(K^*) = -\left(\frac{3}{10\pi}\right)^{1/2},$$

$$F(\Delta) = -\left(\frac{1}{5\pi}\right)^{1/2},$$

where $Y^M_2(K^*$ or $\Delta)$ = spherical harmonic evaluated at K^* or Δ decay angle and $\langle\,\rangle$ means an average over the decay angular distribution.

To describe the quark scattering process there are four independent spin-nonflip and four spin-flip amplitudes. The particle-particle scattering amplitude is the coherent sum of the constituent quark-quark scattering amplitudes.

The tensors can be written in terms of these amplitudes, and if the quantization axis is taken as the production normal we get the following relations:

(I) $\quad T^{20}_{00}(K^*, \Delta) = \sqrt{2}\; T^{02}_{00}(K^*, \Delta),$

(II) $\quad T^{22}_{20}(K^*, \Delta) = \tfrac{1}{2}T^{20}_{20}(K^*, \Delta),$

(III) $\quad T^{22}_{02}(K^*, \Delta) = \dfrac{1}{\sqrt{2}}T^{02}_{02}(K^*, \Delta),$

(IV) $\quad T^{02}_{00}(K^*, \Delta) = \dfrac{1}{2\sqrt{6}} - \dfrac{1}{\sqrt{2}}T^{02}_{00}(K^*, \Delta).$

Since II and III are in general complex, there are six equations. We have combined all data at four momenta: 1.81, 1.94, 2.07, and 2.17 GeV/c. The results are shown in Table XIII and indicate rather good agreement. Figure 22 shows a summary of the test of these relations up to 5 GeV/c.[15] The values of the tensors are rather independent of momentum, and in all cases the equalities appear to be well satisfied.[17]

TABLE XIII. Test of quark-model predictions for the reaction $K^+p \to K^{*0}\Delta^{++} \to K^+\pi^-\pi^+$ evaluated in the transverse helicity frame.

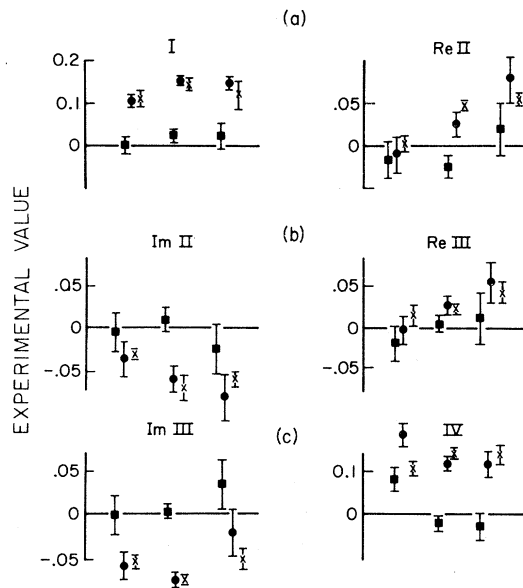| Equation	Left side	Right side	Difference
I	0.104 ± 0.013	0.105 ± 0.027	-0.001 ± 0.030
Re II	-0.012 ± 0.023	0.006 ± 0.006	-0.018 ± 0.023
Im II	-0.040 ± 0.022	-0.034 ± 0.005	-0.006 ± 0.023
Re III	0.003 ± 0.021	0.020 ± 0.010	-0.017 ± 0.023
Im III	-0.062 ± 0.021	-0.057 ± 0.010	-0.005 ± 0.024
IV	0.177 ± 0.029	0.100 ± 0.018	0.077 ± 0.034

FIG. 22. Test of quark-model relations at four momenta: (a) 1.8–2.2 GeV/c, this experiment; (b) 2.5–3.2 GeV/c, Ref. 15; (c) 5.0 GeV/c, Ref. 15. The figure shows the difference ■, left side ●, and right side x.

VI. CONCLUSION

We have studied single-pion production and two-pion production in K^+p reactions. We have considered in detail the two reactions

$$K^+p \to K^0p\pi^+ \tag{1}$$

$$\to K^+p\pi^+\pi^-. \tag{4}$$

The cross section for the $K^0p\pi^+$ reaction shows a

smooth falloff with increasing momentum, as had been previously suggested by Bland.[4] This final state shows strong production of the quasi-two-body states $K\Delta$ and K^*N as at lower momenta. There is some evidence of interference between the K^* and Δ channels in at least qualitative agreement with the findings of Bland.

The $pK^+\pi^+\pi^-$ cross section rises rapidly above 1.7 GeV/c, the threshold for $K^*\Delta$ production. About half the events at each momentum correspond to the quasi-two-body channel. This rapid rise in the two-pion production cross section appears to contribute to the second bump noted earlier in the total cross section.

We have studied the production angular distribution and decay properties of the quasi-two-body channels. All the observed features are in agreement with data at higher and lower momenta, indicating the dominance of peripheral mechanisms.

It is impossible from the inelastic reactions alone to place limits on the contribution of direct-channel mechanisms although the smooth momentum dependence seen in all channels suggests such effects are small. Our data on the inelastic reactions do provide additional information on the K^+p interaction and should be useful in resolving some of the ambiguities in phase-shift analyses of elastic scattering and polarization data.[18]

*Work supported in part by the U. S. Atomic Energy Commission. Prepared under Contracts Nos. AT(11-1)-68 and AT(11-1) Gen 10, Project 17 for the San Francisco Office, U. S. Atomic Energy Commission.

†Present address: Laboratory of Nuclear Studies, Cornell University, Ithaca, New York 14850.

‡Present address: Arkon Research Laboratories, 930 Dwight Way, Berkeley, California 94710.

[1] G. Goldhaber et al., Phys. Rev. Letters 9, 135 (1962); R. L. Cool et al., ibid. 17, 102 (1966); R. J. Abrams et al., ibid. 19, 259 (1967); D. V. Bugg et al., Phys. Rev. 168, 1466 (1968); T. Bowen et al., Phys. Rev. D 2, 2599 (1970). Recent measurements have confirmed the structure in the total cross section above 1 GeV/c; R. L. Cool et al., ibid. 1, 1887 (1970).

[2] R. W. Bland et al., Phys. Letters 29B, 618 (1969); A. Bettini et al., ibid. 16, 83 (1965).

[3] S. Kato et al., Phys. Rev. Letters 24, 615 (1970); P. C. Barber et al., Phys. Letters 32B, 214 (1970);

F. C. Erne et al., in Hyperon Resonances-70, edited by E. C. Fowler (Moore, Durham, N. C., 1970), p. 375.

[4] R. W. Bland, Ph.D. thesis, University of California, Berkeley, 1968 (unpublished); R. W. Bland et al., Nucl. Phys. B13, 595 (1969); B18, 537 (1970).

[5] The beam was designed by J. A. Kadyk of LRL for use at the 25- in. chamber and is described in the Bevatron User's Handbook.

[6] F. T. Solmitz et al., Alvarez Group Programming Note P-117, Berkeley, 1965 (unpublished); O. I. Dahl et al., Alvarez Group Programming Note P-126, Berkeley, 1965 (unpublished); O. I. Dahl, Alvarez Group Programming Note P-124, Berkeley, 1965 (unpublished).

[7] A. Bettini et al., Phys. Letters 16, 83 (1965); W. Chinowsky et al., Phys. Rev. 139, B1411 (1965); F. Bomse et al., ibid. 158, 1298 (1967); J. Fisk et al., in Proceedings of the 1962 International Conference on High-Energy Physics at CERN, edited by J. Prentki (CERN, Geneva, 1962), p. 358; E. Boldt et al., Phys.

Rev. 133, B220 (1964).

[8]R. W. Bland, Ph. D. thesis, University of California, Berkeley, 1968 (unpublished); W. Chinowsky et al., (Ref. 7); F. Bomse et al., (Ref. 7).

[9]P. Eberhard and M. Pripstein, Phys. Rev. Letters 10, 351 (1963).

[10]Sun Yin Fung et al., University of California at Riverside Report No. UCR-34 P107-72 (unpublished); G. Gidal et al., Phys. Rev. Letters 23, 994 (1969).

[11]A. D. Brody et al., Phys. Letters 34B, 655 (1971).

[12]L. Stodolsky and J. J. Sakurai, Phys. Rev. Letters 11, 90 (1963).

[13]M. Ferro-Luzzi et al., Nuovo Cimento 49A, 9 (1967); V. G. Lind et al., Nucl. Phys. B14, 1 (1969).

[14]D. Brown, LBL Report No. UCRL-18254, 1968 (unpublished).

[15]W. De Baere et al., Nuovo Cimento 61A, 397 (1969); G. S. Abrams et al., Phys. Rev. D 1, 2433 (1970).

[16]A. Białas and K. Kalewski, Nucl. Phys. B6, 465 (1968).

[17]It has been pointed out by G. Fox, in Phenomenology in Particle Physics, 1971, proceedings of the conference held at Caltech, 1971, edited by C. B. Chiu, G. C. Fox, and A. I. G. Hey (Caltech, Pasadena, 1971), that the data for $KN \rightarrow K^*\Delta$, and for the SU_3 related reactions $\pi N \rightarrow \rho\Delta$ and $\pi N \rightarrow \omega\Delta$, are also in agreement with predictions of simple absorption models. The data do not favor the quark model over the absorption model. Further tests, where the models give different predictions, are necessary to distinguish the two interpretations.

[18]After preparation of this article we became aware of the data of Brunet et al. on single-pion production reactions between 2.11 and 2.72 GeV/c. We include this reference for completeness. R. C. Brunet et al., Nucl. Phys. B37, 114 (1972).

Production of Strangeness-One Bosons in the Mass Interval 1200–1600 MeV*

W. Frati, J. Halpern,† P. Hargis, and G. Snape
University of Pennsylvania, Philadelphia, Pennsylvania 19104

and

W. Carnahan and M. Nussbaum
University of Cincinnati, Cincinnati, Ohio 45221
(Received 20 April 1972)

The production of $S = 1$ bosons in the mass interval 1200–1600 MeV was investigated in 4-GeV/c $\pi p \rightarrow \Lambda + X^0$ reactions using the missing-mass technique. The momentum and direction of the Λ was determined from the observation of its decay proton and pion in wire spark chambers and the measurement of the proton energy in a range telescope. The $K^*(1420)$ is studied along with a 4-standard-deviation peak at a mass of 1368 MeV.

I. INTRODUCTION

We have applied the missing-mass technique to search for strangeness-1 bosons in 3.98-GeV/c $\pi^- + p \rightarrow \Lambda +$ missing-mass reactions. The mass interval 1200–1600 MeV was explored with a mass resolution of 9, 10, and 12 MeV FWHM (full width at half maximum) at missing masses of 1200, 1400, and 1600 MeV, respectively.

This is a desirable channel for the study of K^* production since the diffractive scattering effects which obscure the interpretation of peaks in K^--nucleon reactions in the Q region are suppressed.[1] It also offers the advantage of a better missing-mass resolution since the principal limitation in proton missing-mass experiments is the Coulomb scattering the proton undergoes in escaping the hydrogen target. The Λ presents no such problem since it leaves the target as a neutral particle, and is required to decay outside the hydrogen target.

II. APPARATUS

A. Beam

The incident π^- beam (schematically shown in Fig. 1) is of the standard triple-focused type with a momentum spread of 8%, and is obtained from the external protons of the Bevatron striking a 3-in. Cu target. To define the momentum of a given incident pion to $\pm\frac{1}{4}\%$, a 24-counter hodoscope is placed at the first focus of the beam. The counters are each $\frac{1}{4}$-in. wide and are placed across the horizontal spread of the beam, where the dispersion is ~1.2% per inch. The effects of chromatic aberration and finite size of the external copper target require the measurement of the position and angle of the beam at the second focus to achieve the desired momentum resolution. The beam was designed to give $\frac{1}{3}\%$ FW momentum resolution, but Coulomb scattering brings this up to